Substitutional diffusion of Mg into GaN from GaN/Mg mixture

Yuta Itoh[1], Shun Lu[1], Hirotaka Watanabe[2], Manato Deki[3], Shugo Nitta[2], Yoshio Honda[2], Atsushi Tanaka[2], and Hiroshi Amano[2,3,4]

[1]*Graduate School of Engineering, Nagoya University, Nagoya 464-8603, Japan*
[2]*Institute of Materials and Systems for Sustainability, Nagoya University, Nagoya 464-8601, Japan*
[3]*Venture Business Laboratory, Nagoya University, Nagoya 464-8603, Japan*
[4]*Akasaki Research Centre, Nagoya University, Nagoya 464-8603, Japan*
E-mail: ito.yuta@nagoya-u.jp

We evaluated Mg diffusion into GaN from GaN/Mg mixture. The diffusion depth of Mg increased with diffusion temperature from 1100 °C to 1300 °C, whereas the Mg concentration remained constant at 2–3×10^{18} cm^{-3} independent of temperature. The estimated activation energy for Mg diffusion was 2.8 eV, from which the substitutional diffusion mechanism was predicted. Mg-diffused GaN samples showed p-type conductivity with a maximum hole mobility of 27.7 $cm^2V^{-1}s^{-1}$, suggesting that substitutional diffusion contributes to Mg activation. This diffusion technique can be used to easily form p-type GaN and has potential as a p-type selective doping technique.

Gallium nitride (GaN) is one of the most promising materials for high-power devices owing to its excellent physical properties such as high breakdown field and high saturated electron velocity.[1–3)] It has already been commercialized for lateral devices such as high-electron-mobility transistors, which are expected to become increasingly popular. On the other hand, the technique of fabricating vertical power devices has not been as well established as that of fabricating lateral ones because there are still many unresolved issues specific to GaN.[4)] In particular, the selective formation of p-type GaN (p-GaN) by Mg ion implantation (Mg I/I) is extremely difficult, which is one of the most important issues that should be resolved for device fabrication.

The problem with Mg I/I often reported is the formation of various defects before and after annealing. During Mg I/I, implanted Mg forms large amounts of Ga vacancy (V_{Ga}) and N vacancy (V_N) complex ($V_{Ga}V_N$).[5–6)] Moreover, during annealing at about 1000 °C, these vacancies aggregate to form clusters such as $(V_{Ga}V_N)_3$, which act as carrier trapping and scattering centers.[5–7)] In addition to the formation and clustering of vacancies, implanted Mg segregates and is not adequately activated as an acceptor.[8–9)] Therefore, to control p-type conduction, the repair or suppression of these defects is essential.

Over the past few years, ultrahigh-pressure annealing (UHPA), which can stably anneal GaN at high temperatures by increasing pressure, has attracted considerable attention as an activation

process for Mg-ion-implanted GaN.[10–13] Mg-ion-implanted GaN annealed at 1480 °C under 1 GPa showed excellent p-type conductivity with comparable mobility to p-GaN fabricated by metalorganic vapor-phase epitaxy (MOVPE).[3, 10] This is because annealing at such a high temperature easily repairs defects such as vacancy clusters and Mg-segregation defects.[9,14] Furthermore, the edge termination of the GaN p–n junction by Mg I/I and UHPA has been reported,[15–16] and UHPA has contributed to the development of GaN power devices from the fabrication of the p-GaN region to its application. However, a high-pressure process should be avoided from an industrialization standpoint, and a process that can be completed at atmospheric pressure is desired. As a non-UHPA approach, various Mg I/I techniques, such as channeling, high-temperature, and vacancy-guided implantation techniques, have been reported to suppress the introduction of defects.[17–20] However, as long as ions are implanted, annealing at temperatures lower than 1300 °C does not completely repair defects, and it seems difficult to fully activate Mg without UHPA. Thus, it is valuable to investigate Mg doping methods without Mg I/I.

As an alternative doping method to Mg I/I, the diffusion method is most promising. Here, the diffusion method refers to doping on surfaces containing high dopant concentrations. Pan et al. have obtained p-GaN by vapor-phase diffusion at 1100 °C for 1 h.[21] However, the hole mobility in p-GaN was 13 $cm^2V^{-1}s^{-1}$ at a hole concentration of 3×10^{15} cm^{-3} at room temperature, which is lower than the mobility of about 25–30 $cm^2V^{-1}s^{-1}$ in epitaxially grown p-GaN with a similar hole concentration.[3, 22–23] Additionally, the activation energy (E_a) for Mg diffusion was estimated as 1.3 eV. According to Wahl et al., E_a for Mg interstitial diffusion was estimated as 1.3 eV by a β^- emission channeling technique.[24] This suggests that the mechanism of vapor-phase Mg diffusion is interstitial-dominated diffusion.

For efficient Mg activation, substitutional diffusion should be dominant. The substitutional diffusion needs the following two factors: the introduction of some Ga vacancies and a higher diffusion temperature. The introduced Ga vacancies enhance Mg substitutional diffusion but the amount of vacancies should be “moderate” without the formation of Mg-segregation defects or vacancy clusters. An increase in diffusion temperature is necessary to make substitutional diffusion dominant because E_a for substitutional diffusion is greater than that for interstitial diffusion. As a Mg-diffusion source that has these factors, we focus on a GaN/Mg mixture (MgGaN) layer, which is formed by annealing Mg deposited on GaN at about 800 °C in nitrogen atmosphere.[25–26] During this annealing, not only Mg diffuses from the Mg layer into the GaN layer, but Ga also diffuses from the GaN layer into the Mg layer.[25] This suggests that Ga vacancies are introduced into the GaN layer. According to Wang et al., most of the Mg that diffused into the GaN layer is not activated,[26] but if the diffusion temperature is further increased, the Mg in the introduced Ga vacancies is likely to be activated; fortunately, the diffusion temperature can be easily increased by depositing a protective film such as AlN on MgGaN. In this paper, we report the Mg diffusion process for p-type GaN formation using MgGaN and the

evaluation of Mg-diffused GaN.

Unintentionally doped Ga-polar GaN (UID-GaN) was grown on n-type freestanding GaN substrates with dislocation densities of about 2×10^6 cm^{-2} by MOVPE. Carbon, oxygen, hydrogen, and silicon in UID-GaN are at background levels or lower than 10^{16} cm^{-3}. A 50-nm-thick Mg layer was deposited on UID-GaN by electron beam deposition [Fig. 1(a)]. GaN with Mg was annealed at 800 °C for 5 min in nitrogen atmosphere at 1 atm. A MgGaN layer and an unintended MgO layer were formed by this annealing [Fig. 1(b)]. The MgO layer was removed with hydrofluoric acid. A 300-nm-thick AlN protective film was deposited by MOCVD at 500 °C to suppresses the decomposition of surface GaN during subsequent annealing [Fig. 1(c)]. GaN layers covered with MgGaN and AlN were annealed at 1100, 1200, and 1300 °C for 1 and 5 min, respectively, in 1 atm nitrogen atmosphere. The MgGaN and AlN layers were removed by immersing the samples in tetramethyl ammonium hydroxide (TMAH) at 80 °C for 2 h [Fig. 1(d)]. In this paper, the first annealing at 800 °C and the subsequent diffusion annealing above 1100 °C are referred to as pre-annealing and drive-in, respectively. The temperature (T) and duration (t) progressions of drive-in are shown in Fig. 1(e). Mg and H concentrations were evaluated by secondary ion mass spectroscopy (SIMS) from the frontside. The diffusion coefficients of Mg were calculated from the SIMS profile.

Figures 2(a) and 2(b) show the Mg concentrations after drive-in at various temperatures for 5 and 1 min, respectively. Figure 2(a) also shows H concentrations. The Mg distribution can be divided into two regions: region I, shallower than about 80 nm from the surface, and region II, the region deeper than region I. In region I, Mg concentrations were higher than those in region II and ranged up to about 10^{20} cm^{-3}; the exact Mg concentration near the surface could not be determined since the SIMS measurements were performed from the frontside containing a high Mg concentration. Region I shows a similar Mg distribution to the MgGaN layer, which is annealed at 800 °C for 5 min, in Ref. 26. Therefore, region I is considered to be the MgGaN layer or region strongly affected by the MgGaN layer. In region II, Mg concentrations remained constant at $2–3\times10^{18}$ cm^{-3} independent of drive-in temperature and duration, whereas Mg diffused deeper into the GaN layer with increasing drive-in temperature and duration. Mg in region II diffused from region I, but the gradient of concentration in region II was smaller than that in region I, indicating that the diffusion mechanisms of regions I and II are different. In only one sample after drive-in at 1100 °C for 1 min, an atypical Mg distribution was observed in region II at depths from 150 to 450 nm. This atypical Mg distribution was observed in multiple measurements but showed no reproducibility, which may be a measurement problem.

In region I, the H concentration is partially as high as the Mg concentration [Fig. 2(a)]. Mg reacts well with H_2O, and the H in region I probably originates from the unintentional moisture on the surface during pre-annealing. Similar results were reported in Ref. 25, which shows the H concentration in MgGaN. On the other hand, the H concentration in region II also correlates with the Mg concentration, but H is below 10 % relative to Mg at any depth. The relationship between H and

Mg is contrary to previous reports. In epitaxially grown p-GaN, H is 100 % relative to Mg because the formation energy of Mg–H complexes is lower than that of Mg on Ga sites.[23, 27] In Mg-implanted p-GaN after UHPA, Mg–H-related diffusion has also been reported; H contamination is attributed to unintentional moisture in high-pressure atmosphere.[11] Thus, in this experiment, Mg diffusion is considered to be different from Mg–H-related diffusion, although the cause of the correlation between H and Mg is unclear. In the later discussion, it is assumed that Mg diffusion is not induced by H.

To determine the Mg diffusion mechanism, Mg diffusion coefficients of regions I and II were calculated. We refer to the dominant diffusion mechanisms in regions I and II as mechanisms I and II, respectively. In the calculations for each mechanism, Fick's Eq. (1) was numerically solved:

$$\frac{\partial C(x,t)}{\partial t} = \frac{\partial}{\partial x}\left(D\frac{\partial C(x,t)}{\partial x}\right) \quad , \qquad (1)$$

where D is the diffusion coefficient and C is the concentration. The boundary conditions were set to maintain a constant level of the Mg-diffusion source from the MgGaN layer $[C(x_0,t) = C_s]$ and zero Mg concentration at points much farther away $[C(\infty,t) = 0]$. x_0 is defined by the Mg-peak point of SIMS profiles and C_s is the constant surface concentration. As for mechanism I, since the topmost-surface concentration in SIMS profiles is not accurate, diffusion coefficients could not be obtained. For the calculation of mechanism II, because a simple Fick's Eq. (1) could not reproduce the experimental values, Eq. (2) was introduced to the calculation [28–29]:

$$D = D_s\left(\frac{C}{C_s}\right)^{\gamma} \quad , \qquad (2)$$

where D_s is the diffusion coefficient at the surface (x_0) and γ shows the concentration dependence. Equation (2) is used when the diffusion coefficient varies with the dopant concentration. In this calculation, γ = 1 was applied. Figure 3 shows the calculated and experimental values of the sample after drive-in for 5 and 1 min. Diffusion coefficients were fitted from SIMS profiles. The calculated values of mechanism II correspond to the experimental values. However, the region with a Mg concentration below 10^{17} cm^{-3} could not be reproduced by calculation under all conditions; a different diffusion mechanism may occur near the diffusion edge.

Figure 4 shows the temperature dependence of the diffusion coefficient for mechanism II. The diffusion coefficient increased exponentially, and the pre-exponential factors D_0 and E_a of mechanism II were estimated as

$$D = D_0 exp\left(-\frac{E_a}{kT}\right) \quad , \qquad (3)$$

where k is the Boltzmann constant and T is the drive-in temperature. E_a and D_0 were estimated as 2.8 eV and 2.8×10^{-3} cm^{2}s^{-1}, respectively. There are many experimental and simulation reports on the relationship between the E_a and diffusion mechanism of Mg in GaN, which are summarized as follows: E_a of interstitial diffusion is less than 1.3 eV and that of substitutional diffusion is more than 1.9 eV.[21,

[24, 26, 29–33] Although this classification does not consider whether it is Mg or Mg–H diffusion, the high E_a of 2.8 eV suggests a substitutional diffusion mechanism.

The dominance of substitutional diffusion in GaN implies that Mg and Ga vacancies are substitutionally diffused. Moreover, in Fig. 4, the measured and calculated Mg diffusion coefficients in this experiment (red circles and line, respectively) are much higher than those in the other fabrication methods such as MOVPE, vapor-phase diffusion, and I/I.[21, 30, 34–35] The substitutional diffusion related to Ga vacancies and the considerably high diffusion coefficient may lead to excessively high Ga vacancy concentrations and their evolution into defects that inhibit Mg activation. To evaluate Mg activation in this experiment, Hall-effect measurements were performed at 27 °C, and all samples were found to show p-type conductivity. In particular, the carrier concentration and hole mobility of the sample after drive-in at 1300 °C for 5 min were 6.4×10^{16} cm^{-3} and 27.7 $cm^2V^{-1}s^{-1}$, respectively; the p-GaN depth nm defined as $\sqrt{2Dt}$ is 428. The hole concentration and mobility are similar to those of MOVPE p-GaN with a Mg concentration of 3.2×10^{18} cm^{-3},[22] which proves that diffused Mg is activated as an acceptor. Therefore, the Ga vacancies, which are assumed to be involved in substitutional diffusion, are not involved in the formation of defects that inhibit Mg activation. Rather, from the observed high Mg activation, the Ga vacancies likely contribute to Mg activation on Ga sites. Such Ga vacancies are considered to be introduced into region I during pre-annealing for MgGaN formation. This is because pre-annealing formed not only a Mg source, but also Ga vacancies in region I of the GaN layer; Ga easily diffuses outward, and the formation of Ga vacancies has also been observed when Al_2O_3 or SiO_2 is deposited and annealed on GaN.[25, 36–37] In the subsequent drive-in, Ga vacancies and Mg seem to diffuse into region II from region I, and the condition of Ga vacancies may be ideal for the diffusion and activation of Mg.

In summary, we have established a Mg diffusion technique using MgGaN for p-type doping. Mg diffused at temperatures of 1100–1300 °C for 1 and 5 min. The diffusion depth of Mg increased with diffusion temperature, whereas the Mg concentration remained constant at $2–3\times10^{18}$ cm^{-3} independent of temperature. E_a for Mg diffusion was estimated as 2.8 eV, suggesting that substitutional diffusion is dominant. Moreover, Mg-diffused GaN samples showed distinct p-type conductivity with a maximum hole mobility of 27.7 $cm^2V^{-1}s^{-1}$, which proves that diffused Mg is activated as an acceptor. Thus, this Mg diffusion technique can be used to easily form p-type GaN, and the temperature required for p-type formation is expected to be significantly reduced; the reduction in temperature facilitates the annealing process at atmospheric pressure. Although the Mg diffusion technique using MgGaN requires further investigation, it has excellent potential as a selective p-GaN fabrication technique.

Acknowledgments

This work was supported by the MEXT Program for Creation of Innovative Core Technology for Power Electronics (Grant Number JPJ009777) and the Ministry of the Environment “Project to

accelerate the social implementation and spread of components and materials to achieve innovative CO_2 reductions (development and verification of a direct current grid system using high-efficiency universal power conditioners)".

References

1) T. Maeda, T. Narita, S. Yamada, T. Kachi, T. Kimoto, M. Horita, and J. Suda, J. Appl. Phys. **129**, 185702 (2021).
2) H. Fujikura, T. Konno, T. Kimura, Y. Narita, and F. Horikiri, Appl. Phys. Lett. **117**, 012103 (2020).
3) T. Narita, K. Tomita, Y. Tokuda, T. Kogiso, M. Horita, and T. Kachi, J. Appl. Phys. **124**, 215701 (2018).
4) T. Kachi, Jpn. J. Appl. Phys. 53 100210 (2014).
5) A. Uedono, S. Takashima, M. Edo, K. Ueno, H. Matsuyama, H. Kudo, H. Naramoto, and S. Ishibashi, Phys. Status Solidi B **252**, 2794 (2015).
6) A. Uedono, S. Takashima, M. Edo, K. Ueno, H. Matsuyama, W. Egger, T. Koschine, C. Hugenschmidt, M. Dickmann, K. Kojima, S. F. Chichibu, S. Ishibashi, Phys. Status Solidi B **255**, 1700521 (2018).
7) S. F. Chichibu, K. Shima, K. Kojima, S. Takashima, K. Ueno, M. Edo, H. Iguchi, T. Narita, K, Kataoka, S. Ishibashi and A. Uedono, Jpn. J. Appl. Phys. **58**, SC0802 (2019).
8) A. Kumar, W. Yi, J. Uzuhashi, T. Ohkubo, J. Chen, T. Sekiguchi, R. Tanaka, S. Takashima, M. Edo, and K. Hono, J. Appl. Phys. **128**, 065701 (2020).
9) K. Iwata, H. Sakurai, S. Arai, T. Nakashima, T. Narita, K. Kataoka, M. Bockowski, M. Nagao, J. Suda, T. Kachi, and N. Ikarashi, J. Appl. Phys. **127**, 105106 (2020).
10) H. Sakurai, M. Omori, S. Yamada, Y. Furukawa, H. Suzuki, T. Narita, K. Kataoka, M. Horita, M. Bockowski, J. Suda, and T. Kachi, Appl. Phys. Lett. **115**, 142104 (2019).
11) H. Sakurai, T. Narita, M. Omori, S. Yamada, A. Koura, M. Iwinska, K. Kataoka, M. Horita, N. Ikarashi, M. Bockowski, J. Suda, and T. Kachi, Appl. Phys. Express **13**, 086501 (2020).
12) K. Sierakowski, R. Jakiela, B. Lucznik, P. Kwiatkowski, M. Iwinska, M. Turek, H. Sakurai, T. Kachi, and M. Bockowski, Electronics **9**, 1380 (2020).
13) M. H. Breckenridge, J. Tweedie, P. Reddy, Y. Guan, P. Bagheri, D. Szymanski, S. Mita, K. Sierakowski, M. Bockowski, R. Collazo, and Z. Sitar, Appl. Phys. Lett. **118**, 022101 (2021).
14) A. Uedono, H. Sakurai, T. Narita, K. Sierakowski, M. Borkowski, J. Suda, S. Ishibashi, S. F. Chichibu, and T. Kachi, Scientific Reports **10,** 17349 (2020).
15) M. Matys, T. Ishida, K. Pil Nam, H. Sakurai, K. Kataoka, T. Narita, T. Uesugi, M. Bockowski, T. Nishimura, Jun Suda, Appl. Phys. Express **14**, 074002 (2021).
16) M. Matys, T. Ishida, K. Pil Nam, H. Sakurai, T. Narita, T. Uesugi, M. Bockowski, J. Suda, and T. Kachi, Appl. Phys. Lett. **118**, 093502 (2021).

17) T. Nishimura, K. Ikeda, and T. Kachi, Applied Physics Express **14**, 066503 (2021).
18) K. Shima, R. Tanaka, S. Takashima, K. Ueno, M. Edo, K. Kojima, A. Uedono, S. Ishibashi, and S. F. Chichibu, Appl. Phys. Lett. **119**, 182106 (2021).
19) M. Takahashi, A. Tanaka, Y. Ando, H. Watanabe, M. Deki, M. Kushimoto, S. Nitta, Y. Honda, K. Shima, K. Kojima, S. F. Chichibu, and H. Amano, Jpn. J. Appl. Phys. **59**, 056502 (2020).
20) Y. Itoh, H. Watanabe, Y. Ando, E. Kano, M. Deki, S. Nitta, Y. Honda, A. Tanaka, N. Ikarashi and H. Amano, Applied Physics Express **15**, 021003 (2022).
21) C. J. Pan and G.C. Chi, Solid–State Electron. **43**, 621–623 (1999).
22) M. Horita, S. Takashima, R. Tanaka, H. Matsuyama, K. Ueno, M. Edo, T. Takahashi, M. Shimizu, and J. Suda, Jpn. J. Appl. Phys. **56**, 031001 (2017).
23) K. Ohnishi, Y. Amano, N. Fujimoto, S. Nitta, H. Watanabe, Y. Honda, and H. Amano, J. Cryst. Growth **12**, 566-567 (2021).
24) U. Wahl, L. M. Amorim, V. Augustyns, A. Costa, E. David-Bosne, T. A. L. Lima, G. Lippertz, J. G. Correia, M. R. da Silva, M. J. Kappers, K. Temst, A. Vantomme, and L. M. C. Pereira, Phys. Rev. Lett. **118**, 095501 (2017).
25) S. Lu, M. Deki, J. Wang, K. Ohnishi, Y. Ando, T. Kumabe, H. Watanabe, S. Nitta, Y. Honda, and H. Amano, Appl. Phys. Lett. **119**, 242104 (2021).
26) J. Wang, S. Lu, W. Cai, T. Kumabe, Y. Ando, Y. Liao, Y. Honda, Y. H. Xie, and H. Amano, IEEE Electron device lett. **43**, 150 (2022).
27) A. Castiglia, J. -F. Carlin, and N. Grandjean, Appl. Phys. Lett. 98, 213505 (2011).
28) L. R. Weisberg and J. Blanc, Phys. Rev. **131**, 1548 (1963).
29) K. Köhler, R. Gutt, J. Wiegert, and L. Kirste, J. Appl. Phys. **113**, 073514 (2013).
30) Z. Benzarti, I. Halidou, Z. Bougrioua T. Boufaden, and B. El Jani, Journal of Crystal Growth **310** 3274–3277 (2008).
31) K. Harafuji, T. Tsuchiya, and K. Kawamura, Phys. Stat. Sol. C **0**, 2240 (2003).
32) K. Harahuji, T. Tsuchiya, and K. Kawamura, Jpn. J. Appl. Phys. **43**, 522 (2004).
33) G. Miceli and A. Pasquarello, Phys. Status Solidi RRL **11**, 1700081 (2017).
34) T. Narita, H. Sakurai, M. Bockowski, K. Kataoka, J. Suda and T. Kachi, Appl. Phys. Express **12** 111005 (2019).
35) S. Porowski, I. Grzegory, D. Kolesnikov, W. Lojkowski, V. Jager, W. Jager, V. Bogdanov, T. Suski and S. Krukowski, J. Phys.: Condens. Matter **14,** 11097 (2002).
36) A. Uedono, T. Nabatame, W. Egger, T. Koschine, C. Hugenschmidt, M. Dickmann, M. Sumiya, and S. Ishibashi, J. Appl. Phys. **123**, 155302 (2018).
37) A. Uedono, W. Ueno, T. Yamada, T. Hosoi, W. Egger, T. Koschine, C. Hugenschmidt, M. Dickmann, and Heiji Watanabe, J. Appl. Phys. **127**, 054503 (2020).

Figure captions

Fig. 1 (Color online) (a)–(d) Mg diffusion process. (e) Temperature and duration progressions of drive-in.

Fig. 2 (Color online) Depth profiles of Mg concentrations at various drive-in temperatures for (a) 5 and (b) 1 min obtained by SIMS. (a) also shows H concentrations.

Fig. 3 (Color online) Depth profiles of Mg after drive-in at various temperatures for 5 and 1 min, and calculated curves of various drive-in conditions.

Fig. 4 (Color online) Diffusion coefficients obtained in this work and previous study. The red line shows Arrhenius Eq. (3), where E_a and D_0 are 2.8 eV and 2.8×10^{-3} cm^2s^{-1}, respectively.

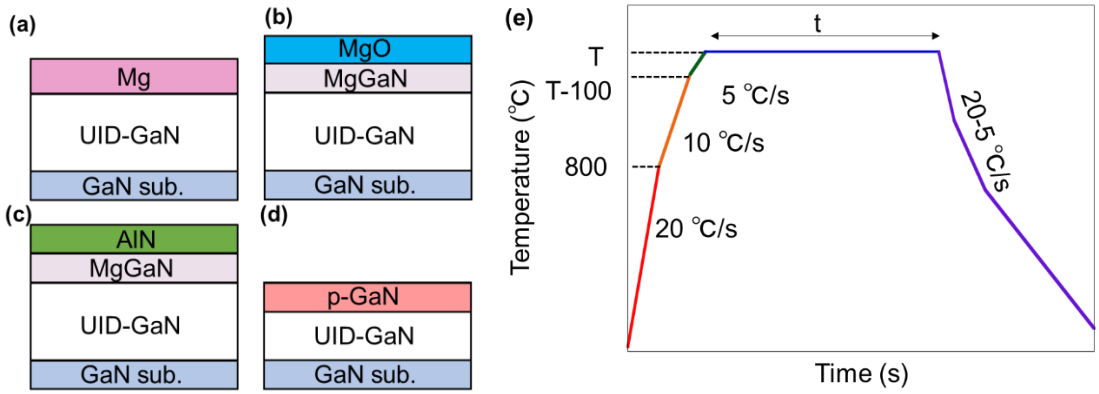

Fig. 1

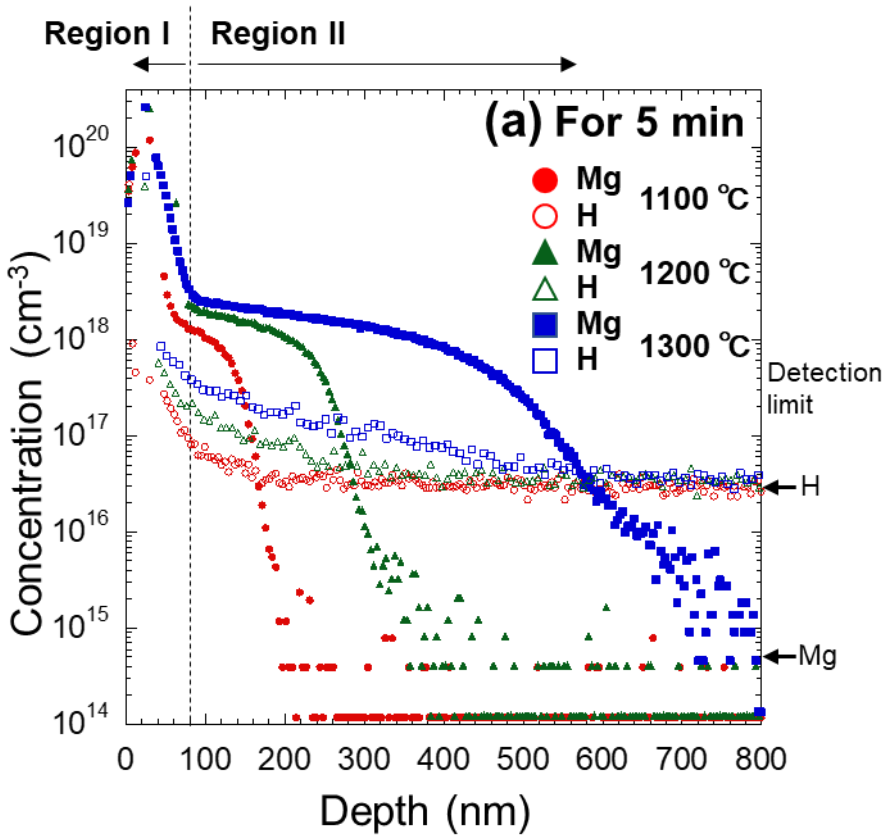
Region I
Region II
(a) For 5 min
Mg
H
1100 ℃
Mg
H
1200 ℃
Mg
H
1300 ℃
Detection limit
H
Mg
Concentration (cm-3)
Depth (nm)

269

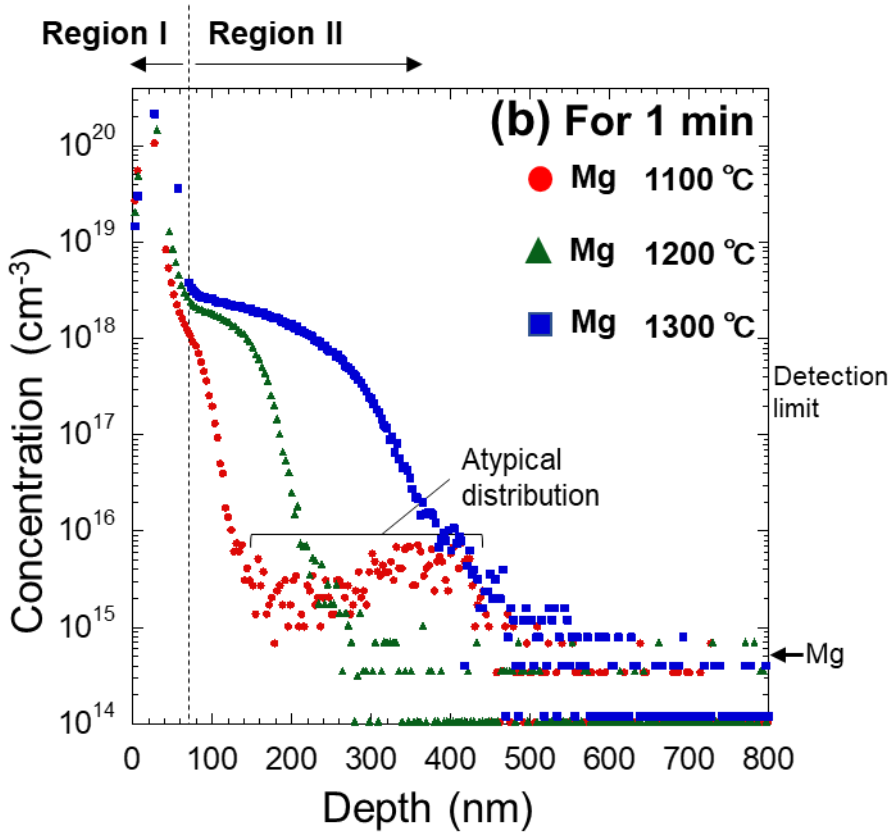
Region I
Region II
(b) For 1 min
Mg
1100 ℃
Mg
1200 ℃
Mg
1300 ℃
Detection limit
Atypical distribution
Mg
Concentration (cm-3)
Depth (nm)

270

Fig. 2

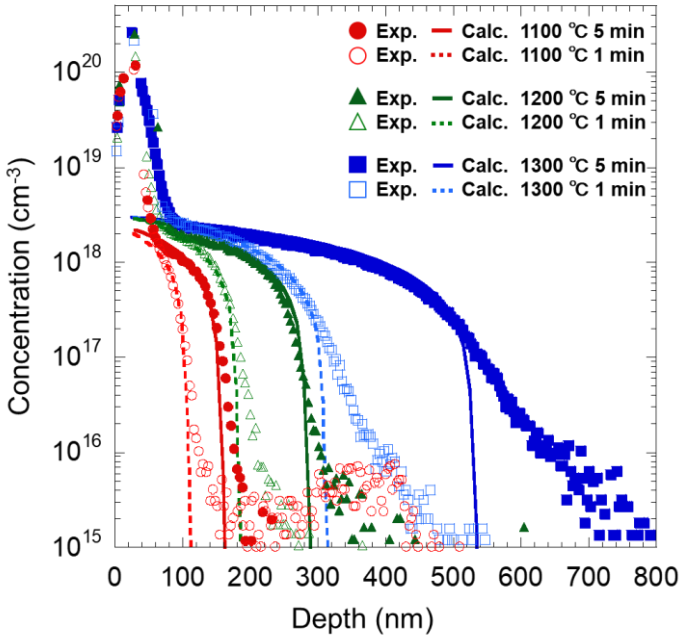

Fig. 3

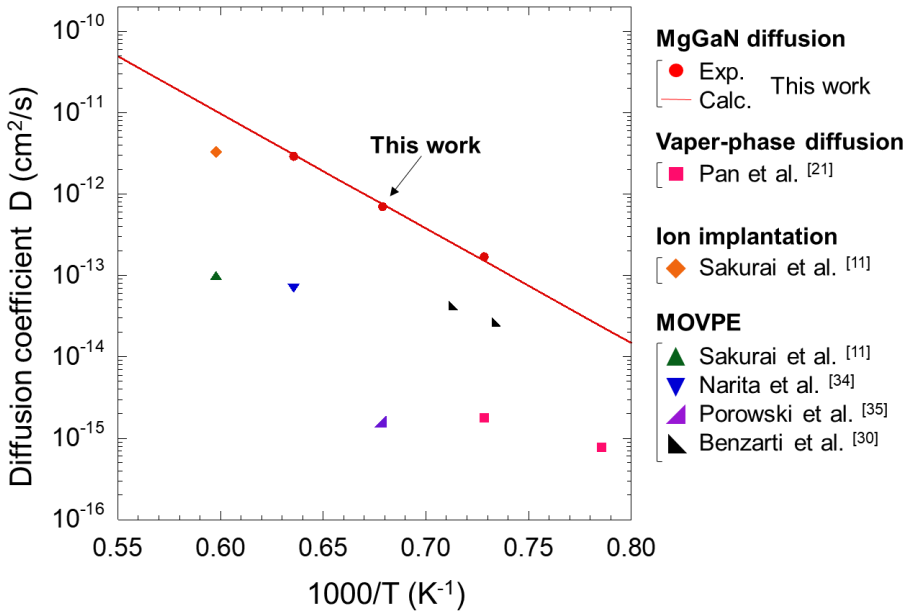

Fig. 4